Effects of nonuniform viscosity on ciliary locomotion

Kourosh Shoele[1] and Patrick S. Eastham[2]
[1]*Department of Mechanical Engineering, Florida State University, Tallahassee, Florida 32310, USA*
[2]*Department of Mathematics, Florida State University, Tallahassee, Florida 32304, USA*

(Received 30 October 2017; published 24 April 2018)

The effect of nonuniform viscosity on the swimming velocity of a free swimmer at zero Reynolds number is examined. Using the generalized reciprocal relation for Stokes flow with nonuniform viscosity, we formulate the locomotion problem in a fluid medium with spatially varying viscosity. Assuming the limit of small variation in the viscosity of the fluid as a result of nonuniform distribution of nutrients around a swimmer, we derive a perturbation model to calculate the changes in the swimming performance of a spherical swimmer as a result of position-dependent viscosity. The swimmer is chosen to be a spherical squirmer with a steady tangential motion on its surface modeling ciliary motion. The nutrient concentration around the body is described by an advection-diffusion equation. The roles of the surface stroke pattern, the specific relationship between the nutrient and viscosity, and the Péclet number of the nutrient in the locomotion velocity of the squirmer are investigated. Our results show that for a pure treadmill stroke, the velocity change is maximum at the limit of zero Péclet number and monotonically decreases toward zero at very high Péclet number. When higher surface stroke modes are present, larger modification in swimming velocity is captured at high Péclet number where two mechanisms of thinning the nutrient boundary layer and appearance of new stagnation points along the surface of squirmer are found to be the primary reasons behind the swimming velocity modifications. It is observed that the presence of nonuniform viscosity allows for optimal swimming speed to be achieved with stroke combinations other than pure treadmill.

DOI: 10.1103/PhysRevFluids.3.043101

I. INTRODUCTION

Many cellular microorganisms, both prokaryotic and eukaryotic, use some types of self-propulsion mechanisms to move through their surrounding environment [1–4]. In most cases, the viscous stress is the dominant locomotive force in microorganism swimming and inertial effects are negligible [4–6]. Therefore, for microorganisms to propel themselves through the surrounding environment, they use non-time-reversible types of motion [7]. The nonreversible swimming kinematics are usually associated with wavylike beating motion of flexible slender appendages attached to the surface of a microorganism, known as either flagella or cilia, depending on their length relative to the size of the organism. While many microorganisms have a small number of very long flagella, such as eukaryotic flagella in mammalian spermatozoa [1,8–10], other organisms, such as Paramecium, possess many shorter ciliates over the cell surface to create the required thrust for locomotion [1]. The latter mode of swimming is called ciliary locomotion.

As a microorganism swims, it creates flow features that could affect the transport of nutrients near its surface [11–14]. In particular, the metabolism of many microorganisms relies on the absorption of other molecules, cells, or particles at their surfaces which, for convenience in this paper, are all referred to as a nutrient [15]. A nutrient, which could be low-weight molecules, dissolved gases, complex proteins, or even heat, are transported by diffusion and advection processes of the flow which themselves are caused by the motion of single or multiple organisms, or even external factors.

There is a strong correlation between the transport of nutrients and swimming kinematics used by microorganisms, which is a vital feature in survival of large microorganisms [1,16]. The relative importance of advection versus diffusion mechanisms in the transport of nutrients around a swimmer is characterized by the nutrient Péclet number [12–14]. At small Péclet number, diffusion is dominant and therefore the nutrient concentration is anticipated to be homogeneous. At high Péclet number, the advection transport from the flow that is created by the motion of the swimmer surface is dominant. In this case, the nutrient concentration changes rapidly in the radial direction across a thin boundary layer near the surface of a microorganism.

The rate of nutrient intake at the surface of a swimmer not only affects the growth and reproduction rate of a microorganism [17–19], it can also modify the swimming speed of the organism or even enables an originally nonmotile system to start moving [20]. The depletion of certain chemical agents from the surface of a microorganism or cell can also modify the material properties of fluid near the body by varying its effective viscosity and/or viscoelasticity; experimentalists have primarily used two compounds, methyl cellulose and Foxin, to systematically change the bulk viscosity of a medium [21,22]. These are long-chain polymers and, while not being digestible, do suggest that other long-chained nutrients, such as complex sugars and proteins, could have a similar effect on bulk viscosity. Here we assume that a nutrient-dependent bulk viscosity can be extended to a theoretical pointwise-dependence.

This model of swimming has been explored for microrobots and has been successfully employed in different bioinspired applications [23]. For example, an artificial, miniaturized, chemically powered body can react chemically to the surrounding flow and creates asymmetric chemical agent distribution around the swimmer that causes a finite-amplitude fluid velocity near the surface of the body and consequently allows the body to propel itself in its surrounding environment. This mode of swimming, which is essentially caused by the slip boundary condition on the surface of a body, is known as phoretic swimming [24,25]. A similar situation is also observed for a spherical chemical droplet at the interface of two media where an asymmetric distribution of a chemical agent at the contact line of the droplet and the interface leads to a net Marangoni force on the droplet and results in a finite swimming velocity of this force-free body [26–29]. A similar Marangoni force has been seen for solid bodies that are asymmetrically heated [30–33]. All of these locomotion modes have an origin in the changes in the fluid boundary conditions at the surface of a swimmer. This leads to the question of what would happen when a nutrient modifies the properties of near-body fluid, even though the fluid boundary conditions at the surface of the swimmer are unaffected? There have been several recent experimental [34,35] and theoretical [36–40] studies into how swimming efficiency is affected by non-Newtonian flows with shear-dependent viscosities. Non-Newtonian fluid models have the added benefit of taking into account more realistic physics, including both memory effects due to the fluid elasticity and the fluid viscosity modification due to the shear stress, at the cost of increasing the model complexity. Nganguia *et al.* [39] suggested that there is an optimal shear rate for swimmers with the squirmer model of locomotion at which the swimming efficiency can be substantially enhanced in fluids with shear-thinning viscosities compared with the Newtonian case. The swimming performance in non-Newtonian fluids highly depends on the ratio between the fluid relaxation and flow characteristic time scales, known as the Deborah number, as well as other interconnecting effects such as self-propulsion modes [37,38]. As a model problem, in this study, a straightforward case of a Newtonian fluid with nutrition-dependent viscosity is assumed to investigate the effect of nutrient consumption on the swimming velocity.

The distribution of nutrients around a cell can change extracellular plasma viscosity or viscoelasticity directly or indirectly. While a bacteria suspension has been shown experimentally to decrease a fluid's net bulk viscosity [41], the manipulation of local nutrient gradients by two specific bacteria will help illustrate a primary mechanism of this type of microorganism's motility. *H. pylori* is an ulcer-causing flagellar microorganism that lives in the highly acidic environment of human stomachs. It has been found that this organism moves through the thick gel-like environment by releasing urease, a substance which increases the *p*H of the gastric mucus fluid. This benefits the motility of *H. pylori* by changing the local fluid properties around its surface and modifies the force acting on the cell

body [42]. Recent theoretical work has been done to determine the environmental constraints for *H. pylori*'s motility [43]. *Synechococcus* is a cyanobacteria that obtains its nutrients through oxygenic photosynthesis. Although it has no flagella or cilia, it is mysteriously able to swim through liquid suspensions [44,45]. It is still an open question as to how it generates propulsion; many studies have been done to examine possible swimming modes [46,47], and experimental studies have ruled some out, such as electrophoresis [48]. However, one hypothesis is that modification of near-surface nutrient concentration is the reason behind their swimming abilities. We are thus motivated to study the potential connection between the local changes in the nutrient concentration and its effect on the locomotion speed of a free swimmer with potential applications for developing next generation, efficient, artificial biomimetic microswimmers [49]. In this mode of locomotion, the absorption of nutrients on the surface of a cell results in reduction of their concentrations and in turn modifies the pointwise viscosity of fluid near the surface of the swimmer. The purpose of the present paper is to investigate this mechanism and determine to what extent the viscosity change around a mobile microorganism affects the swimming performance of the body.

We employ the generalized Lorentz reciprocal theorem [50] to relate the problem with nonuniform viscosity to the counterpart problem with uniform viscosity. Using a reciprocal theorem is a popular technique which has been successfully used in other fluids problems [51,52]. By solving for the nutrient concentration in an advection-diffusion process around a free swimmer inside a fluid with uniform viscosity [12,13], we quantify the changes in the swimming velocity of the body when it moves in a fluid domain with nonuniform viscosity. To obtain the fluid velocity and stress, we also need to model the Stokes flow near the swimmer. This problem is primarily affected by viscous effects and the locomotion performance of the system only depends on the sequence of shapes used by the swimmer and not on the rate of shape changes [4,5]. Solving for rate-independent flow field around a general free-swimming cell is challenging, especially when the swimmer shape is complex with many appendages like flagella or cilia. Different techniques have been proposed to study these kinds of systems. The most common are the boundary element method [53], simplified techniques like regularized Stokeslets [54], slender boundary theory [4,55], or the use of fundamental singularities [56] to impose boundary conditions on the surface of a swimmer. Because they consider general shapes, these methods are inherently complicated to implement and generally are computationally expensive. One may use an alternative approach and approximate the geometry of a swimmer with a simplified canonical shape and solve the Stokes equation exactly in the uniform viscosity domain. This approach allows exploring the effects of a wide range of controlling parameters on the hydrodynamics of force-free bodies at the limit of zero-Reynolds-number flow. This approach has been used successfully to study different mechanisms related to the hydrodynamics of ciliated swimmers [57,58].

In this study we employ the latter approach and focus on the spherical squirming swimmer for which the exact solution for uniform viscosity Stokes flow is available and has been used in previous studies [59–62]. The mathematical model of a spherical squirmer can be considered as a simplified representation of ciliated microorganisms [57,58] and is routinely used to study individual and collective dynamics of these microorganisms. Here we decompose the stroke motion at the surface of a spherical swimmer into swimming and nonswimming modes and explore how each stroke mode affects the swimming velocity through modification of near-field viscosity as a result of nutrient uptake at the surface.

The rest of the paper is organized as follows. In the next section we define the physical problem and present the mathematical formulation, including the governing equations and the mathematical solutions, and define the key characteristic quantities for the analysis. The results are then presented and conclusions are drawn.

II. MATHEMATICAL FORMULATION

The swimmer is assumed to be a spherical ciliate at a very small Reynolds number $\mathrm{Re} = \rho U R/\mu \sim 0$, where U is the characteristic velocity, R is the radius of the swimmer, and ρ and

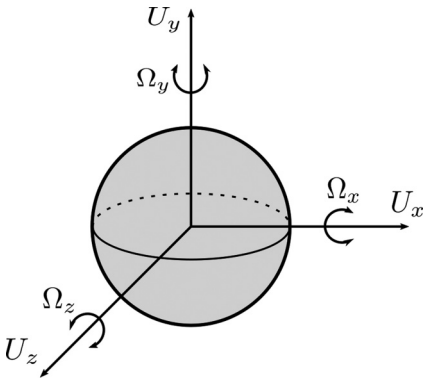

FIG. 1. Sketch of translational $\boldsymbol{U}$ and rotational $\boldsymbol{\Omega}$ terms for our canonical shape.

μ are, respectively, the mass density and dynamic viscosity of the surrounding fluid. The surface of the swimmer moves with a given velocity $\mathbf{u}^s$ measured from a body-fixed coordinate system. At very small Reynolds number, the fluid velocity field $\mathbf{u}$ is approximated by the Stokes equations

$$\nabla \cdot \underline{\boldsymbol{\sigma}} = \nabla \cdot (-p\underline{\boldsymbol{I}} + 2\mu\underline{\boldsymbol{E}}) = 0, \quad \nabla \cdot \mathbf{u} = 0, \tag{1}$$

where $\underline{\boldsymbol{E}} = \frac{1}{2}(\nabla\mathbf{u} + \nabla\mathbf{u}^\top)$ is the rate-of-deformation tensor, $\underline{\boldsymbol{\sigma}}$ is the Newtonian stress tensor, and μ is the spatially varying viscosity. In addition, the boundary conditions at the surface of body and far field are, respectively,

$$\mathbf{u} = \mathbf{u}^s + (\boldsymbol{U} + \boldsymbol{\Omega} \times \mathbf{x}) \quad \text{at } r = R, \quad \boldsymbol{u} \to 0 \quad \text{as } r \to \infty, \tag{2}$$

where $\boldsymbol{U} = (U_x, U_y, U_z)$ and $\boldsymbol{\Omega} = (\Omega_x, \Omega_y, \Omega_z)$ are the transitional and rotational velocities of a swimmer and are determined through imposing the free-swimming boundary conditions on the surface of the swimmer (see Fig. 1)

$$\int_S \boldsymbol{\tau}\, ds = 0, \quad \int_S \mathbf{x} \times \boldsymbol{\tau}\, ds = 0,$$

where $\boldsymbol{\tau} = \mathbf{n} \cdot \underline{\boldsymbol{\sigma}}$ is the traction on the boundary, and $\mathbf{n}$ is the unit normal vector to the surface of the swimmer S, and $\mathbf{x}$ is the position vector.

We assume that the swimmer is placed in a nutrient solution with far-field concentration of C_0. We follow previous studies by Magar *et al.* [12] and Michelin and Lauga [13] and assume that the nutrient is completely absorbed at the surface of the swimmer, i.e., $C = 0$ at $r = R$. The distribution of C is further assumed to be governed by the steady advection-diffusion equation

$$\mathbf{u} \cdot \nabla C = \kappa \nabla^2 C, \quad C = 0 \quad \text{at } r = R, \quad C \to C_0 \quad \text{as } r \to \infty, \tag{3}$$

where κ is the nutrient diffusion coefficient and $\mathbf{u}$ is the fluid velocity found by Stokes equations (1) and (2).

The viscosity of extracellular plasma is assumed to be nonuniform and directly related to the pointwise nutrient concentration in the flow according to

$$\mu = \mu_0 + k\mu_0 \left(\frac{C_0 - C}{C_0} \right)^{\xi}, \tag{4}$$

where k and ξ are dimensionless coefficients characterizing the nature of viscosity change for different types of nutrients. Qualitatively, $k > 0$ is for the cases in which the reduction of a nutrient increases the viscosity, like in the case of heat absorption by a swimmer, and $k < 0$ is for the situation in which the reduction of a nutrient decreases the viscosity, as is the case of glucose and proteins. The exponential form is for our desire to qualitatively capture experimentally determined nutrient-dependent bulk

viscosity, seen best in Fig. 1 of [22]. Assuming that the change in the fluid viscosity is small, we can define $k = \epsilon$ with the assumption that $\epsilon \ll 1$ and use ϵ for the scale separation in perturbation analyses described in Sec. II A. Equation (4) then can be rewritten as

$$\mu(\mathbf{x}) = \mu_0 + \epsilon\mu_1(\mathbf{x}), \quad \mu_1(\mathbf{x}) = \mu_0\left(\frac{C_0 - C(\mathbf{x})}{C_0}\right)^{\xi}. \tag{5}$$

The changes in the swimming speed of an organism are related to the distribution of nonuniform viscosity μ_1 through the reciprocal theorem as explained in Sec. II A.

A. Generalized reciprocal theorem for Stokes flow

In order to calculate the swimming velocity of an organism, a generalized reciprocal theorem (GRT) is utilized to relate the current problem to a similar problem with the same geometry but uniform viscosity. The derivation for viscous flow follows straightforwardly from [50], so details are left to Appendix A. The integral form of the GRT is

$$\iint_S \mu\mathbf{U}\cdot\boldsymbol{\tau}'ds + \iint_S \mu\Omega\cdot(\mathbf{x}\times\boldsymbol{\tau}')ds + \iint_S \mu\mathbf{u}^s\cdot\boldsymbol{\tau}'ds = -\iiint_V \nabla\mu\cdot\underline{\boldsymbol{\sigma}}'\cdot\mathbf{u}\,dv, \tag{6}$$

where the prime denotes fields in our auxiliary constant viscosity domain, which for our spherical swimmer will be defined later in Eqs. (11) and (12). From Eq. (5) we can expand all velocity fields in Eq. (6) in a regular perturbation series, e.g., $\mathbf{u} = \sum_m \epsilon^m\mathbf{u}_m$, and obtain the $O(\epsilon^0)$ term

$$\iint_S \mu_0\mathbf{U}_0\cdot\boldsymbol{\tau}'ds + \iint_S \mu_0\Omega_0\cdot(\mathbf{x}\times\boldsymbol{\tau}')ds + \iint_S \mu_0\mathbf{u}^s\cdot\boldsymbol{\tau}'ds = 0. \tag{7}$$

Knowing that μ_0, $\mathbf{U}_0$, and Ω_0 are constants, Eq. (7) simplifies to

$$\mathbf{U}_0\cdot\mathbf{F}' + \Omega_0\cdot\mathbf{T}' = -\iint_S \mathbf{u}^s\cdot\boldsymbol{\tau}'ds, \tag{8}$$

where $\mathbf{F}' = \iint_S \boldsymbol{\tau}'ds$ is the total force acting on the swimmer and $\mathbf{T}' = \iint_S \mathbf{x}\times\boldsymbol{\tau}'ds$ is the resultant fluid dynamic torque on the body. The relation is a classical problem solved originally by Stone and Samuel [63]. In a similar way, we can write the $O(\epsilon^1)$ relation as

$$\begin{aligned}&\iint_S \mu_0\mathbf{U}_1\cdot\boldsymbol{\tau}'ds + \iint_S \mu_0\Omega_1\cdot(\mathbf{x}\times\boldsymbol{\tau}')ds + \iint_S \mu_1\mathbf{U}_0\cdot\boldsymbol{\tau}'ds + \iint_S \mu_1\Omega_0\cdot(\mathbf{x}\times\boldsymbol{\tau}')ds\\ &+ \iint_S \mu_1\mathbf{u}^s\cdot\boldsymbol{\tau}'ds = -\iiint_V \nabla\mu_1\cdot\underline{\boldsymbol{\sigma}}'\cdot\mathbf{u}_0 dv.\end{aligned} \tag{9}$$

Since μ_1 is constant on S from Eqs. (3) and (5), the summation of the last three terms on the left-hand side of Eq. (9) is zero from Eq. (7) and therefore Eq. (10) can be transformed to

$$\mathbf{U}_1\cdot\mathbf{F}' + \Omega_1\cdot\mathbf{T}' = -\iiint_V \frac{\nabla\mu_1}{\mu_0}\cdot\underline{\boldsymbol{\sigma}}'\cdot\mathbf{u}_0 dv. \tag{10}$$

The above derivation is valid for Stokes flow with nutrient-dependent viscosity in *any* geometry. The next step for the current problem is to define an auxiliary Stokes problem and solve for $(\mathbf{U}_0,\Omega_0)$ and $(\mathbf{U}_1,\Omega_1)$ using Eqs. (8) and (10). Since in this paper we are interested in axisymmetric motion of a spherical squirmer, we set $\Omega_0 = \Omega_1 = 0$ and choose a translational motion of a sphere of radius R with the velocity of $\mathbf{U}'$ along the x axis in a fluid with constant viscosity of μ_0 and no surface deformation as an auxiliary flow problem. The solution of this classical problem is well known and

its velocity fields in the body-centered coordinate system can be written as

$$u_i' = \frac{1}{4}R\left[3\frac{\delta_{ij}}{r} + 3\frac{x_i x_j}{r^3} + R^2\left(\frac{\delta_{ij}}{r^3} - \frac{3x_i x_j}{r^5}\right)\right]U_j', \tag{11}$$

$$\sigma_{ij}' = -\frac{3}{2}\mu_0 R\left[3\frac{x_i x_j x_k}{r^5} + R^2\left(\frac{\delta_{ij}x_k + \delta_{jk}x_i + \delta_{ki}x_j}{r^5} - 5\frac{x_i x_j x_k}{r^7}\right)\right]U_k', \tag{12}$$

which results in $\mathbf{F}' = -6\pi\mu_0 R\mathbf{U}'$ and $\mathbf{T}' = \mathbf{0}$. This allows the simplification of Eqs. (8) and (10) into

$$\mathbf{U}_0 = -\frac{1}{4\pi R^2}\iint_S \mathbf{u}^s dS, \tag{13}$$

$$\mathbf{U}_1 \cdot \mathbf{F}' = -\iiint_V \frac{\nabla\mu_1}{\mu_0} \cdot \underline{\boldsymbol{\sigma}}' \cdot \mathbf{u}_0 dv. \tag{14}$$

Equation (13) is the zeroth-order swimming velocity which only depends on the stroke pattern used by a swimmer. Similarly, the first-order change of the swimming velocity is given by Eq. (14). However, to calculate the right-hand side of Eq. (14), we should remember that $\mu_1 = \mu_1(C)$, so the nutrient field is required in the fluid domain around the swimmer. A related point to consider is that Eq. (10) only provides the first-order correction to the swimming velocity while ignoring higher-order effects. In particular, the $O(\epsilon^1)$ changes of the flow field causes up to $O(\epsilon^1)$ modification in the nutrient field, which then induces up to an $O(\epsilon^2)$ correction to μ in Eq. (5). Thus, for the limit of small viscosity changes on the order of ϵ, we only need to include the one-way coupling between the nutrient concentration and the flow field in order to calculate the first-order velocity correction and disregard the higher-order effects caused by the changes of the nutrient field as a result of modified flow velocities. Toward this, we use the squirmer model to solve for the fluid domain and nutrient distribution around a swimmer. The formulation and numerical procedure are explained in Sec. II B.

The resultant flow equations are nondimensionalized using the radius of the swimmer R as the length scale and $\sqrt{RQ/\mu_0}$ as the time scale where $Q = -\iint_S \mathbf{u}^s \cdot \boldsymbol{\tau}' ds$ is the rate of work performed by the swimmer against the surrounding fluid with uniform constant viscosity. Hereafter, we consider nondimensional forms of our equations and use the same notation for the nondimensional quantities as their dimensional counterparts.

B. Model of squirming motion of a sphere

In the squirming model, we consider the body-fixed coordinate system with the origin at the center of a sphere. The swimmer is considered to have a translational motion $\boldsymbol{U} = (-U_x, 0, 0)$ pointing towards the negative side of the x axis. A spherical coordinate system is employed to describe the flow field using r and $\gamma = \cos(\theta)$ for radial and polar coordinates, respectively, where θ is the angle between the $\mathbf{r}$ vector and the positive direction of the x axis. The surface of the swimmer is located at $r = 1$ and its velocity is purely tangential, i.e., $\mathbf{u}^s = u_\theta^s \mathbf{e}_\theta$. We can fully characterize u_θ^s using a Legendre polynomial series [12,13,57] as

$$u_\theta^s(\gamma) = \sum_{n=1}^{\infty} \beta_n K_n(\gamma), \tag{15}$$

where $K_n(\gamma) = \sqrt{\frac{3}{n(n+1)}}\sqrt{1-\gamma^2}P_n'(\gamma)$, with P_n being the Legendre polynomial of order n. Here β_n specifies the contribution of the mode n in the swimming stroke. From the previously explained nondimensionalization procedure based on the rate of energy dissipation [13,57], β_n is normalized

such that it satisfies

$$\frac{2}{3}\beta_1^2 + \sum_{n=2}^{\infty} \beta_n^2 = 1. \tag{16}$$

When the viscosity of fluid is constant, the first mode with $n = 1$ defines the swimming velocity and it is possible to show that $\beta_1 = \sqrt{\frac{3}{2}}U$. Other modes are not swimming modes and only contribute to local flow features near the body. Previous studies have shown that the maximum propulsion speed by a swimmer inside uniform viscosity fluid for a constant energy expenditure occurs when the surface velocity of the swimmer is made of only the first stroke mode ($\beta_n = \delta_{1,n}$).

Since the Stokes problem is linear, the flow field can also be generated by a superposition of solutions of different swimming modes. This allows the stream function ψ of the flow to be defined as

$$\psi(r,\gamma) = \sum_{n=1}^{\infty} \beta_n \Psi_n(r,\gamma), \tag{17}$$

where

$$\Psi_n(r,\gamma) = \frac{1-\gamma^2}{\sqrt{n(n+1)/3}} P_n'(\gamma)\phi_n(r), \tag{18}$$

$$\phi_n(r) = \begin{cases} \frac{1-r^3}{3r} & \text{if } n = 1 \\ \frac{1}{2}\left(\frac{1}{r^n} - \frac{1}{r^{n-1}}\right) & \text{if } n > 1. \end{cases} \tag{19}$$

The fluid velocity can then be computed from

$$\mathbf{v} = -\frac{1}{r^2}\frac{\partial \psi}{\partial \gamma}\mathbf{e}_r - \frac{1}{r\sqrt{1-\gamma^2}}\frac{\partial \psi}{\partial r}\mathbf{e}_\theta, \tag{20}$$

where $\mathbf{v}$ is the fluid velocity measured from the body-fixed coordinate system and is related to the actual fluid velocity through $\mathbf{u} = \mathbf{v} - U\mathbf{e}_x$.

Defining the nondimensional nutrient deficit as $c = \frac{C_0 - C}{C_0}$, the nondimensional form of Eq. (3) in a spherical coordinate system is

$$\frac{1}{\mathrm{Pe}}\left[\frac{\partial}{\partial r}\left(r^2\frac{\partial c}{\partial r}\right) + \frac{\partial}{\partial \gamma}\left((1-\gamma^2)\frac{\partial c}{\partial \gamma}\right)\right] = \sum_{n=1}^{\infty}\beta_n\left[\frac{\partial \Psi}{\partial r}\frac{\partial c}{\partial \gamma} - \frac{\partial c}{\partial r}\frac{\partial \Psi}{\partial \gamma}\right], \tag{21}$$

with the near- and far-field boundary conditions of

$$c(1,\gamma) = 1, \quad c(\infty,\gamma) = 0. \tag{22}$$

In Eq. (21), $\mathrm{Pe} = \frac{1}{\kappa}\sqrt{QR/12\pi\mu_0}$ is the Péclet number which compares the advective and diffusive transport rates at the surface of the swimmer. Equations (21) and (22) are used to calculate the effects of each mode of the stroke, e.g., β_i, on the nutrient concentration. To solve for c, we follow the method previously proposed in [64] and subsequently used in [12,13] and rewrite c with its Legendre polynomial series expansion in the γ direction as

$$c(r,\gamma) = \sum_{j=1}^{\infty} c_j(r)P_j(\gamma). \tag{23}$$

This results in a coupled linear system of equations for different Legendre polynomial terms. The resultant equation for the coefficient of the P_j term in Eq. (23) can be written explicitly as

$$\mathrm{Pe}\sum_{n=1}^{\infty}\sum_{m=0}^{\infty}\beta_n\left[A_j(m,n)\frac{dc_m}{dr}\psi_n + B_j(m,n)c_m\frac{d\psi_n}{dr}\right] = \frac{d}{dr}\left(r^2\frac{dc_j}{dr}\right) - j(j+1)c_j, \tag{24}$$

with the boundary conditions

$$c_j(1) = \delta_{j1}, \quad c_j(\infty) = 0. \tag{25}$$

The coupling coefficients $A_j(m,n)$ and $B_j(m,n)$ can be calculated by utilizing the recurrence properties of Legendre polynomials and are given in Appendix B.

The finite-difference method is employed to discretize Eq. (24) in the radial direction. To achieve higher grid density near the body, a stretched grid in the r direction is used through mapping a uniformly spaced N_r grid in ζ ($1 \leqslant \zeta \leqslant \zeta_{\max}$) to the radial direction with $r = e^{\zeta}$. Our numerical sensitivity tests show that $N_r = 700$ and $\zeta_{\max} = 10$ are sufficient to accurately capture the thin boundary layer of c at the surface of the swimmer at the highest tested Pe (here limited to $\mathrm{Pe} = 600$) and also reduce the effects of domain truncation at the far-field at the limit of very small Pe number.

The Legendre polynomial series in Eqs. (23) and (24) is truncated after $j = J$ and only the first J modes of the Legendre polynomial are retained. Our sensitivity analyses show that $J = 400$ is sufficient to accurately resolve the concentration field in the azimuthal direction in the most sensitive cases with very high Péclet number. In addition, we also assume that the squirming motion of the surface of the swimmer can be described by the first 12 Legendre polynomials and therefore the summation in Eq. (15) is truncated at $N = 12$.

III. RESULTS

The methodology described in the preceding section is employed to calculate the change in the swimming velocity of the squirmer for different Pe and ξ as a result of surface motion with a combination of stroke mode shapes β_i. To quantify the effects of viscosity change on the swimming velocity of a microorganism, we define $cm(r,\gamma) = \frac{\xi c^{\xi-1}}{U_0 F'}\nabla c \cdot \sigma' \cdot \mathbf{u}_0$ to be the kernel of Eq. (14) (e.g., $U_1/U_0 = -\int_V cm\, dv$), which physically represents to what extent spatially varying nutrient concentration around the swimmer affects the swimming velocity. We will go into detail about the effects of the nutrient gradient and Pe for the pure treadmill case and then describe how multiple swim strokes together affect the swimming performance in different environments.

A. Pure treadmill motion with $\beta_i = \sqrt{\frac{3}{2}}\delta_{1i}$

In Figs. 2(a)–2(d) the concentration fields of c and cm are shown for four values of Pe (0.02, 1, 50, and 500, respectively) around a swimmer with pure treadmill stroke $\beta_i = \sqrt{\frac{3}{2}}\delta_{1i}$, the $\sqrt{3/2}$ needed to keep the overall power expended normalized. When Pe is very low [Fig. 2(a)], the nutrient concentration is isotropic and decays similarly in the r direction at every γ value, which results in a very weak asymmetry between the front and back of the swimmer. The contour plot of cm has two primary areas with large values, a very confined region at the side of the swimmer where cm shows its maximum values and thus has a negative effect on the first-order swimming velocity change U_1/U_0, and two very similar and relatively larger regions, around $|\gamma| \geqslant 0.8$, where cm attains its minimum value and therefore increases U_1/U_0.

At higher Pe [starting with $\mathrm{Pe} = 1$ in Fig. 2(b)], the front-back symmetry breaks, resulting in a larger region with negative cm to appear in the front of the organism rather than its back. At the same time, as the concentration boundary layer near the side of the swimmer becomes thinner, a region with large positive cm value appears. The overall effect is an increase in U_1/U_0 compared to smaller-Pe-number problems.

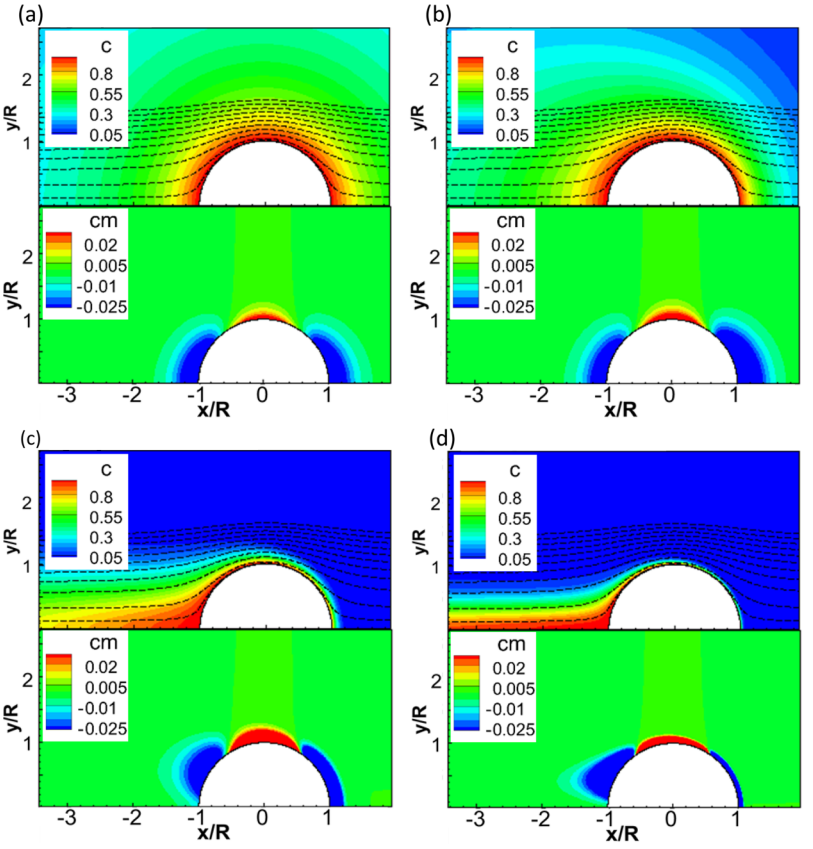

FIG. 2. Contour plots of nutrient concentration c and its effect cm on U_1/U_0 around a spherical swimmer with the pure treadmill squirming surface motion ($\beta_i = \sqrt{3/2}\delta_{1i}$) for (a) Pe $= 0.02$ and $U_1/U_0 = 0.084$, (b) Pe $= 1$ and $U_1/U_0 = 0.102$, (c) Pe $= 50$ and $U_1/U_0 = 0.073$, and (d) Pe $= 500$ and $U_1/U_0 = 0.032$. The dashed lines are the streamlines for each case.

As Pe increases [Figs. 2(c) and 2(d)], stronger angular asymmetry appears in the nutrient concentration around the squirmer where the boundary layer of nutrient becomes thin in front of the swimmer and a confined wake emerges behind the squirmer. Figures 2(b)–2(d) show that the region with a large positive value of cm at the side of the organism is stronger in the case of Pe $= 50$ compared to higher and lower Péclet numbers of Pe $= 500$ and 1. The reduction in thickness of the nutrient boundary layer at the side of the squirmer is the reason for the reduction in U_1/U_0 at Pe $= 500$ compared to Pe $= 50$. Moreover, the most dominant region with negative values of cm shifts from the front of the swimmer at Pe $= 1$ to the back at Pe $= 50$ and 500. At very high Pe, here Pe $= 500$, this region appears to become smaller and primarily concentrated in a thin boundary layer near the surface of the swimmer except very close to $\gamma = -1$, where the boundary layer depletes into the wake behind the swimmer.

The results of Fig. 2 suggest that there is a range of Pe with maximum influence on the swimming velocity. To better understand the effects of the parameters on the swimming velocity of the squirmer, the contour plot of U_1/U_0 of a swimmer with a pure treadmill surface stroke is shown in Fig. 3 for $10^{-3} \leqslant \text{Pe} \leqslant 600$ and $0.25 \leqslant \xi \leqslant 4$. In addition, the asymptotic values of U_1/U_0 at Pe $\gg 1$ and Pe $\ll 1$ are also shown with dashed and dash-dotted lines, respectively. The analytical asymptotic formulations of U_1/U_0 are calculated from the behavior of (21) at very large and very small Péclet numbers, as discussed in Appendixes C and D. Overall, very good agreement is found between

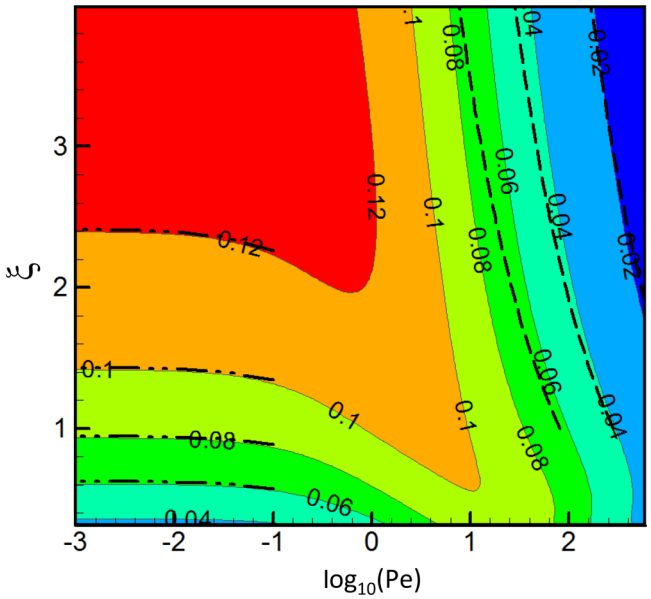

FIG. 3. Dependence of the first-order swimming velocity of the squirmer U_1/U_0 on $\log_{10}(\mathrm{Pe})$ and ξ for the pure treadmill motion $\beta_i = \sqrt{\frac{3}{2}}\delta_{i1}$. Dashed contour lines are the asymptotic results for $\mathrm{Pe} \gg 1$. Similarly, dash-dotted contour lines correspond to the asymptotic results for very low Pe.

the numerical results and the asymptotic values at extreme values of Pe, which also validates the numerical method.

From Fig. 3 it can be seen that for the tested ranges of ξ and Pe values, U_1/U_0 is positive and, depending on the sign of ϵ or equivalently the nature of viscosity change with nutrient concentration, the swimming performance of the squirmer always monotonically increases or decreases with the changes in the viscosity. The maximum value of U_1/U_0 of more than 0.12 occurs at small Pe and large ξ. For $\mathrm{Pe} < 0.1$, the change in the swimming speed is almost independent of Pe and only depends on ξ; this contrasts greatly with the high-Pe regime, where U_1/U_0 is primarily a function of Pe and monotonically approaches 0 with increasing Pe. This implies that under similar condition, smaller microorganisms are more affected by the changes in the viscosity due to the rate of nutrient consumption than larger microorganisms. However, as will be discussed later, the effect of viscosity change on U_1/U_0 at high-Pe values is highly dependent on the surface stroke pattern, especially if other stroke modes besides the pure treadmill motion are present in the surface motion.

B. Changes in the swimming velocity for different Pe

In this section we explore the effect of Péclet number on the swimming velocity of an organism when the surface velocity consists of two modes: the treadmill mode and one of the higher stroke modes. We only consider the first three higher stroke modes as previous literature has suggested that swimming microorganisms can reasonably be approximated with only the first couple of modes [13].

First it is assumed that the surface motion only consists of the treadmill and the second, third, or fourth stroke mode. While the responses of $\beta_2/\beta_1 = -1$ and 1 [in Figs. 4(a) and 4(d), respectively] are very similar at low Pe, the case of $\beta_2/\beta_1 = -1$ has a local maximum at $\mathrm{Pe} \sim O(1)$, while such feature is not present in the case of $\beta_2/\beta_1 = 1$. Additionally, the asymptotic value of U_1/U_0 at very small Pe numbers approaches zero when $\beta_2/\beta_1 = 1$ and reaches a finite negative value of -0.05 when $\beta_2/\beta_1 = -1$. The cases of $\beta_{3,4}/\beta_1 = \mp 1$ [Figs. 4(b) and 4(e)] show similar behavior, however the peak appears now for the positive ratio at slightly higher Pe. The results shows that the nature

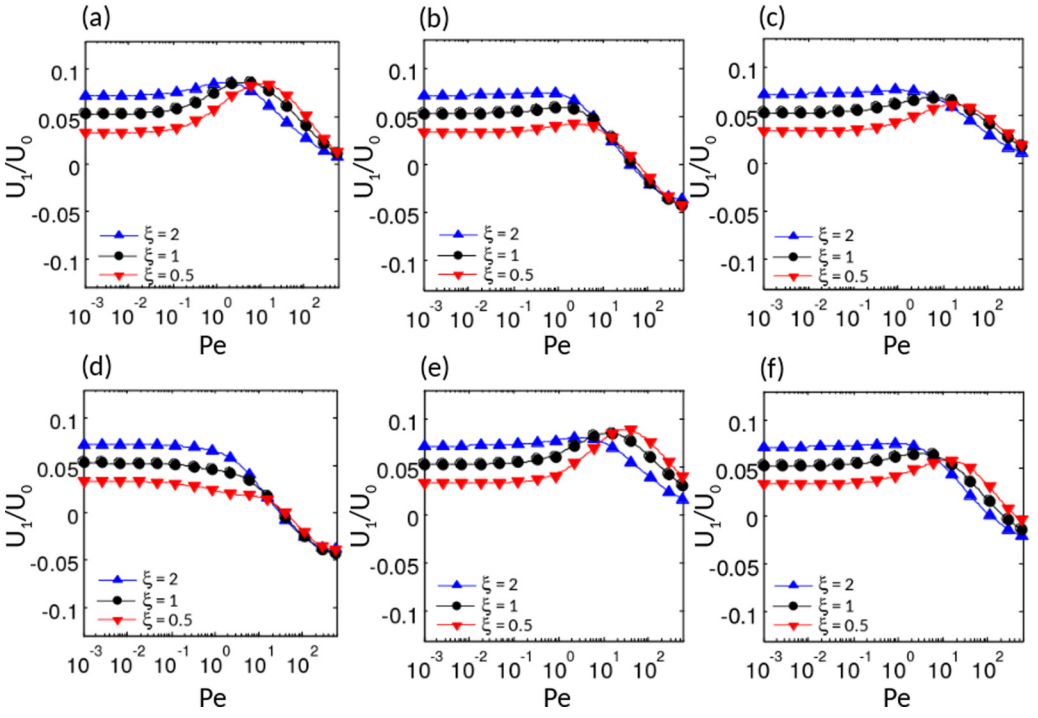

FIG. 4. Dependence of the relative swimming velocity change on the Péclet number for different ξ when the tangential velocity of the organism surface consists of β_1 and β_i, $i = 2,3,4$: (a) and (d) $\frac{\beta_2}{\beta_1} = \mp 1$, (b) and (e) $\frac{\beta_3}{\beta_1} = \mp 1$, and (c) and (f) $\frac{\beta_4}{\beta_1} = \mp 1$.

of the change of U_1 with Pe numbers is highly dependent on the few first squirmer modes; this is in contrast to the higher stroke modes, e.g., Figs. 4(c) and 4(f), where the responses are similar to what has been observed in Fig. 2 for the pure treadmill motion.

The contour plots of c and cm for $\beta_2/\beta_1 = 1$, $\beta_3/\beta_1 = 1$, and $\beta_4/\beta_1 = 1$ near the observed peaks at a Péclet number of Pe $= 50$ are shown in Figs. 5(a), 5(b), and 5(c), respectively. It can be seen that

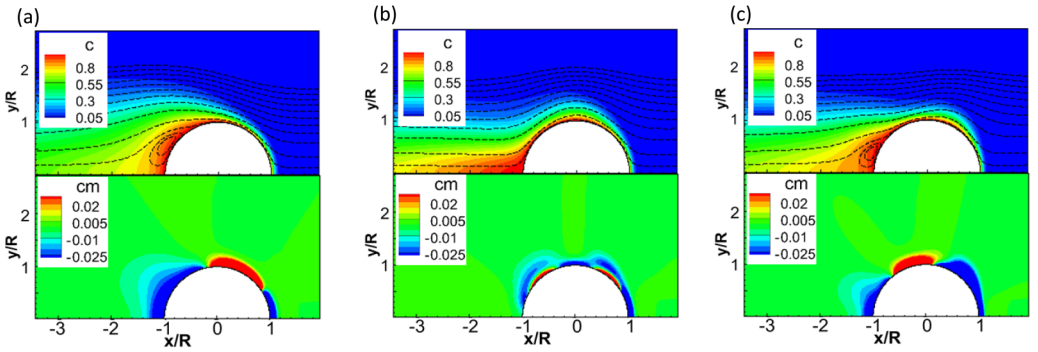

FIG. 5. Distributions of nutrient concentration (top row) and its distributed effect on U_1/U_0 (bottom row) around the spherical swimmer with (a) $\beta_2/\beta_1 = 1$ and $U_1/U_0 = -0.01$, (b) $\beta_3/\beta_1 = 1$ and $U_1/U_0 = 0.074$, and (c) $\beta_4/\beta_1 = 1$ and $U_1/U_0 = 0.033$ at Pe $= 50$ and $\xi = 1$. The streamlines for each surface stroke are shown in the first row of figures.

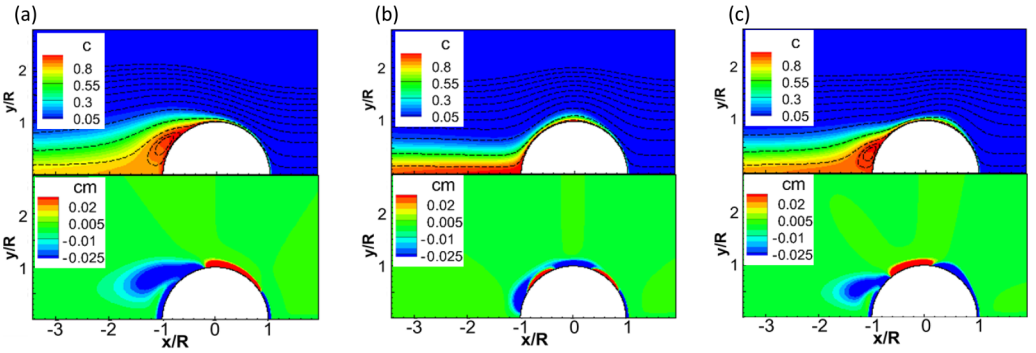

FIG. 6. Similar to Fig. 5 except that Pe = 500 and (a) $U_1/U_0 = -0.042$, (b) $U_1/U_0 = 0.033$, and (c) $U_1/U_0 = -0.012$.

the distribution of c around the swimmer shows a large dependence on the stroke modes used by the squirmer, causing the cm contour plot to differ between stroke cases. In particular, the $\beta_2/\beta_1 = 1$ case shown in Fig. 5(a) has a larger region on top and anterior of the swimmer with positive cm and the negative regions of cm are in a small region behind the swimmer and a much larger region in front of the swimmer. At $\beta_3/\beta_1 = 1$, shown in Fig. 5(b), because of the symmetric motion of the swimmer surface and nearly symmetric distribution of c with respect to the y axis except near $\gamma = \pm 1$, the contour of cm around the swimmer is symmetric. In this case, negative regions grow in size and result in a larger increase of U_1/U_0 than in the similar case at low Pe. From Fig. 5(c) it can be seen that in the case of $\beta_4/\beta_1 = 1$ the dominant negative region of cm switches from the back of the swimmer to its front at $\gamma \sim 0.6$ and the region with positive cm increases in both size and magnitude, resulting in small U_1/U_0.

At very high Pe, Pe = 500 in Fig. 6, the main contribution of the c distribution only concentrates at the boundary layer of the swimmer and the largest value of cm, either positive or negative, happens along the surface of the swimmer. The exception is at isolated stagnation points along the surface motion where the nutrient boundary layer separates. The stagnation points are placed near the back of the squirmer where a larger region with small magnitude of negative cm bursts from the surface and stretches into the wake. The effective consequence of an increase in the strength of the region with positive cm and detachment of the region with negative cm from the surface of the swimmer (where $\underline{\sigma}'$ has a larger value) is a reduction in U_1/U_0 compared to the smaller Pe regime of Pe = 50.

C. Changes in the swimming velocity for coupled β_i

In this section we study how the surface stroke pattern affects the swimming velocity of the squirmer. As we have discussed in the preceding section, the surface stroke pattern is an important factor when Pe $\geqslant 1$ and thus in this section we choose three representative Pe numbers of 1, 20, and 500 and focus only on the dependence of U_1/U_0 on the surface stroke pattern when the squirmer uses the treadmill motion and one of the second to fourth surface modes.

The dependence of U_1/U_0 on $|\beta_i|/\beta_1$ (i is a mode number between 2 and 4) at Pe = 1 is shown in Figs. 7(a)–7(c). Here, except for $|\beta_2|/\beta_1$, the results of positive and negative β_i/β_1 (shown with closed and open symbols, respectively) of other cases are almost identical. In these cases, each ξ curve reaches its constant asymptotic limit of U_1/U_0 at a small ratio of the modes and decays rapidly between $|\beta_i|/\beta_1 = 0.2$ and 10 to become almost zero at higher mode ratios. The region where the curves show their most rapid decay is almost independent of ξ and only depends on the ratio of the higher stroke mode to the treadmill mode. In all cases, U_1/U_0 increases with the increase of the ξ exponent at small $|\beta_i|/\beta_1$ ratios. The exceptional behavior happens at $|\beta_2|/\beta_1 \simeq 1$, where the

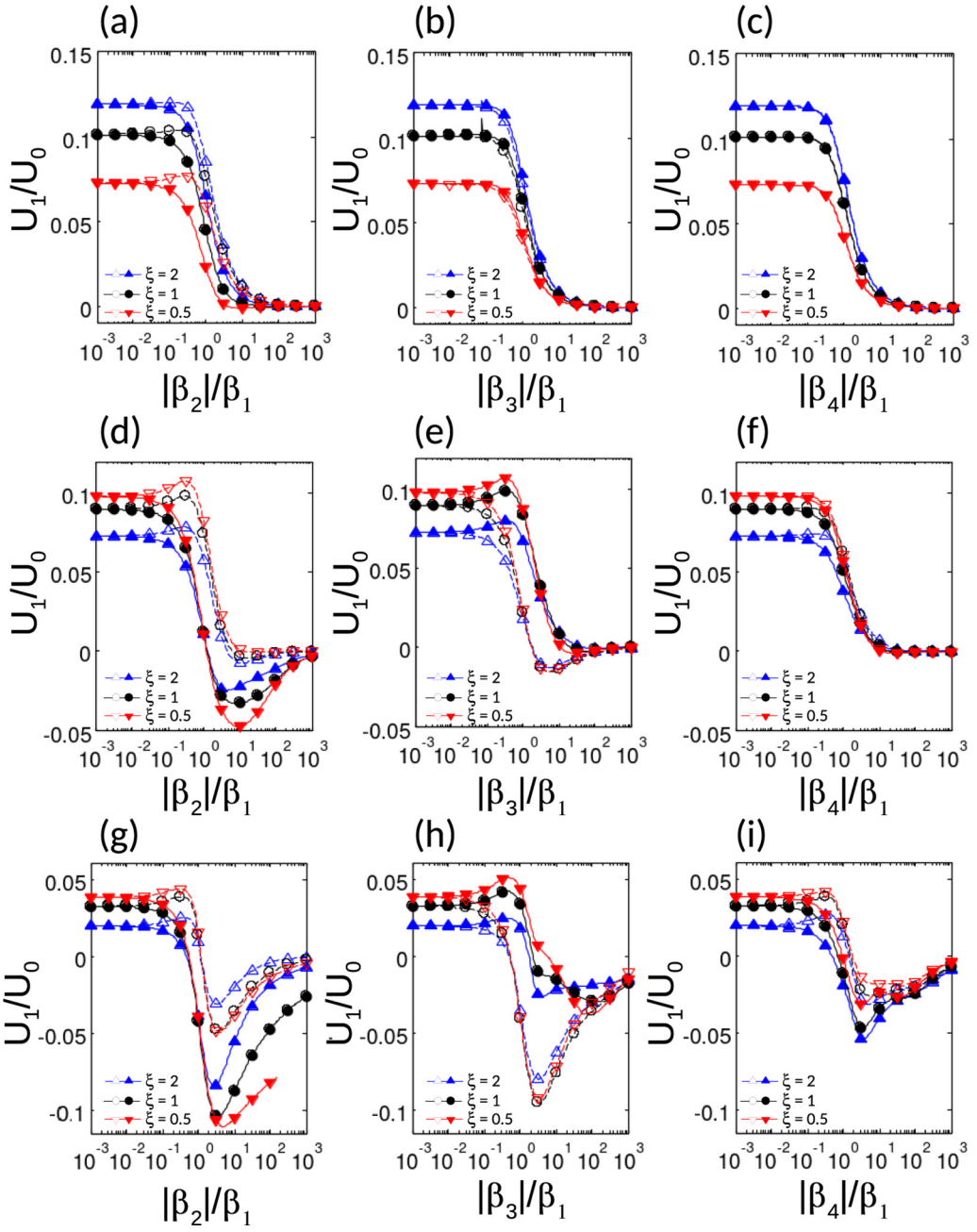

FIG. 7. Dependence of the relative swimming velocity change on the ratio of (a) $|\beta_2|/\beta_1$, (b) $|\beta_3|/\beta_1$, and (c) $|\beta_4|/\beta_1$ for different ξ coefficient at Pe $= 1$; (d) $|\beta_2|/\beta_1$, (e) $|\beta_3|/\beta_1$, and (f) $|\beta_4|/\beta_1$ for different ξ coefficient at Pe $= 20$; and (g) $|\beta_2|/\beta_1$, (h) $|\beta_3|/\beta_1$, and (i) $|\beta_4|/\beta_1$ for different ξ coefficient at Pe $= 500$. In each figure, the surface motion consists of the first and only one of the higher stroke modes. The open symbols are for $\beta_i/\beta_1 < 0$ and closed symbols are for $\beta_i/\beta_1 > 0$. Note the varying scales of the vertical axis.

negative value of β_2 results in a small local rise in U_1/U_0 around $\beta_2/\beta_1 = -1$. Also for this case it is found that the swimmer has a nearly maximum U_1/U_0 unless the amplitude of the second stroke mode becomes larger than the first mode, $\beta_2 \leqslant -\beta_1$.

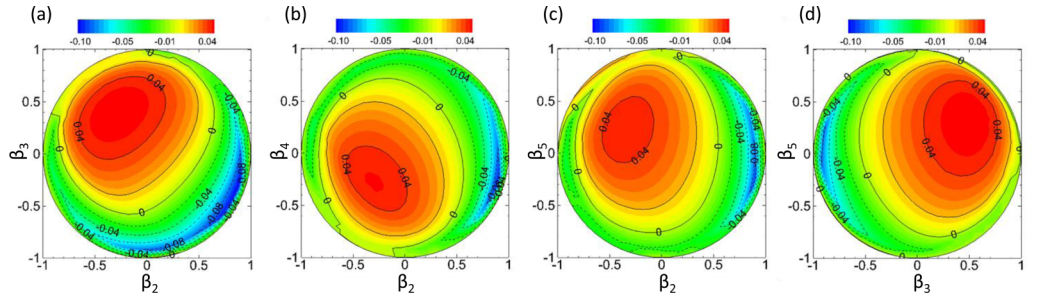

FIG. 8. Changes of the first-order swimming velocity U_1/U_0 in (a) the β_2-β_3 plane and (b) the β_2-β_4 plane, assuming Pe $= 400$. Here β_1 is calculated from $\frac{2}{3}\beta_1^2 + \sum_{i\neq 1}\beta_i^2 = 1$. It is assumed that $\xi = 1$.

When we vary the $|\beta_i|/\beta_1$ ratios over a wide range, we see that, in general, pure treadmill-dominated ($|\beta_i|/\beta_1 \ll 1$) motions give the best swimming performance. However, most interestingly, in certain cases there is a peak maximum for equal ratios, notably for $\beta_2/\beta_1 = O(1)$ and Pe $= 20$. This peak increases as the rate of nutrient change dampens near the cell surface (as opposed to a rapid change with high ξ). An interpretation of this is the need for a boundary layer to generate a front-back asymmetry along the organism. If the boundary layer is large or nonexistent (Pe $\ll 1$) then there is no front-back asymmetry in viscosity to generate a propulsive force, and if the boundary later is too small (Pe $\gg 1$) then no stroke effect is able to propagate in the fluid far enough to substantially affect the swimming velocity. However, it should be noted that for the vast majority of cases, the swimming performance monotonically decreases as $|\beta_i|/\beta_1$ is increased. This lends further evidence towards pure treadmill strokes being optimal.

At Péclet number of Pe $= 20$, shown in Figs. 7(d)–7(f), the U_1/U_0 curves show larger variations with both positive and negative values. In particular, the curves of a positive ratio of the stroke mode in Fig. 7(d) have minimum values at $\beta_2/\beta_1 \simeq 10$. In contrast, the negative β_2/β_1 curves show a localized increase in U_1/U_0 at $\beta_2/\beta_1 = -0.3$ for all ξ values before they decrease rapidly to $U_1/U_0 \simeq 0$ at $\beta_2/\beta_1 < -10$. For the case of $|\beta_3|/\beta_1 \neq 0$ shown in Fig. 7(e), the trend is reversed and the positions of extrema shift slightly compared to Fig. 7(d). Nonetheless, the changes in U_1/U_0 for the combination of the first and third modes are smaller than what has been observed for the combination of the first and second surface stroke modes. Also U_1/U_0 curves of higher surface stroke modes, $|\beta_4|/\beta_1$ in Fig. 7(f), show minor sensitives to the sign of the surface stroke mode.

At high Péclet number of Pe $= 500$, U_1/U_0 shows great sensitivity to the magnitude and sign of β_i/β_1 for all test cases [Figs. 7(g)–7(i)]. Moreover, the smallest U_1/U_0 is observed in all cases at $|\beta_i|/\beta_1 \simeq 3$ for either positive or negative higher stroke modes.

Finally, to see the effects of surface motion with more than two stroke modes, in Fig. 8 the changes of U_1/U_0 within the β_2-β_3, β_2-β_4, β_2-β_5, and β_3-β_5 planes are plotted. In each case, the boundary of search space and the value of β_1 are from the constraint of the invariant consumed energy [Eq. (16)]. Moreover, here we choose $\xi = 1$ and Pe $= 400$. The (0,0) node in each plane corresponds to the pure treadmill mode, which previously had been shown to be both the optimal swimming and optimal feeding scenario [13]. It is observed that the maximum U_1/U_0 does not correspond to the pure treadmill surface stroke and happens for a finite amplitude of higher modes. In particular, when the horizontal axis is β_2, the position of the maximum U_1/U_0 shifts to the negative side of the x axis, and when the horizontal axis is β_3, it moves to the positive side, which is very similar to the trend observed in Fig. 7 when the surface motion consists of only two stroke modes. The place of the maximum U_1/U_0 with respect to the vertical axis depends on the sequence of higher modes. If they are entirely even modes (e.g., $\beta_2, \beta_4, \ldots$) or merely odd modes (e.g., $\beta_3, \beta_5, \ldots$), the maximum of U_1/U_0 corresponds to the case in which both modes have the same sign, but if one of the higher modes is odd and the other is even, the maximum of U_1/U_0 occurs when the modes have opposite signs. The maximum value of U_1/U_0 for these cases is larger and reaches 0.044 compared to $U_1/U_0 = 0.035$

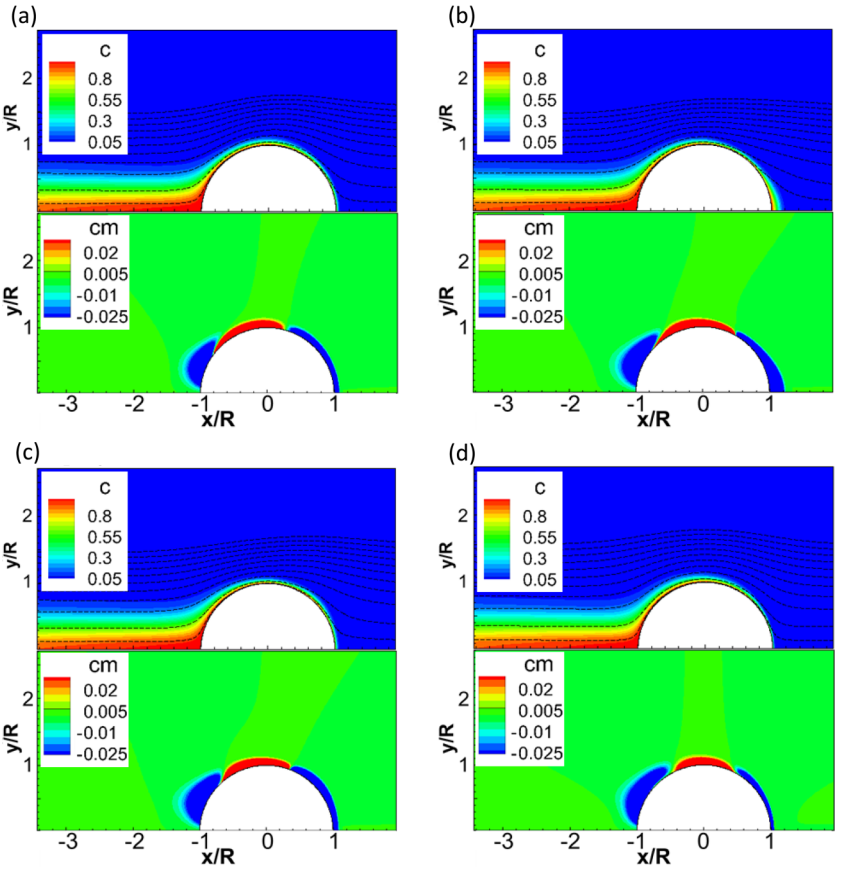

FIG. 9. Distributions of nutrient concentration (top row) and its distributed effect on U_1/U_0 (bottom row) for the maximum observed values in Fig. 7 assuming Pe $= 400$ and $\xi = 1$: (a) point $(-0.296, 0.402)$ in the β_2-β_3 plane for $U_1/U_0 = 0.0487$, (b) point $(-0.307, -0.282)$ in the β_2-β_4 plane for $U_1/U_0 = 0.0456$, (c) point $(-0.356, 0.255)$ in the β_2-β_5 plane for $U_1/U_0 = 0.044$, and (d) point $(0.491, 0.310)$ in the β_3-β_5 plane for $U_1/U_0 = 0.0487$.

in the case with pure treadmill motion. This is evidence for more optimal swimming strokes than just pure treadmill when a nonuniform viscosity environment is considered.

The streamlines and concentration contours of cases corresponding to the maximum U_1/U_0 observed in Fig. 8 are shown in Fig. 9. The combination of the surface stroke modes in these cases makes the constructive cm ($cm < 0$) stronger at the front and back of the swimmer, mainly by increasing the radial gradient of c in those spots. At the same time, the optimal combination of the modes marginally decreases the strength and extent of the destructive cm ($cm > 0$). The unique feature observed for all optimal combinations of higher modes is that the boundary layer stays connected and higher surface stroke modes only marginally modulate the boundary layer of the pure treadmill stroke without inducing any new stagnation point along the surface of the swimmer.

The minimum U_1/U_0 of the cases shown in Fig. 8 is less than -0.081 with the minimum observed value of $U_1/U_0 = -0.097$ corresponding to surface motion of $\beta_1 = 0.454$, $\beta_2 = 0.869$, and $\beta_3 = -0.328$. It is found that the regions with a negative U_1/U_0 value are narrow in the radial direction and elongated in the angular direction.

The contour plots of c and cm for the cases with minimum U_1/U_0 are shown in Fig. 10, where the boundary layer modifies substantially with new stagnation points appearing along the surface of

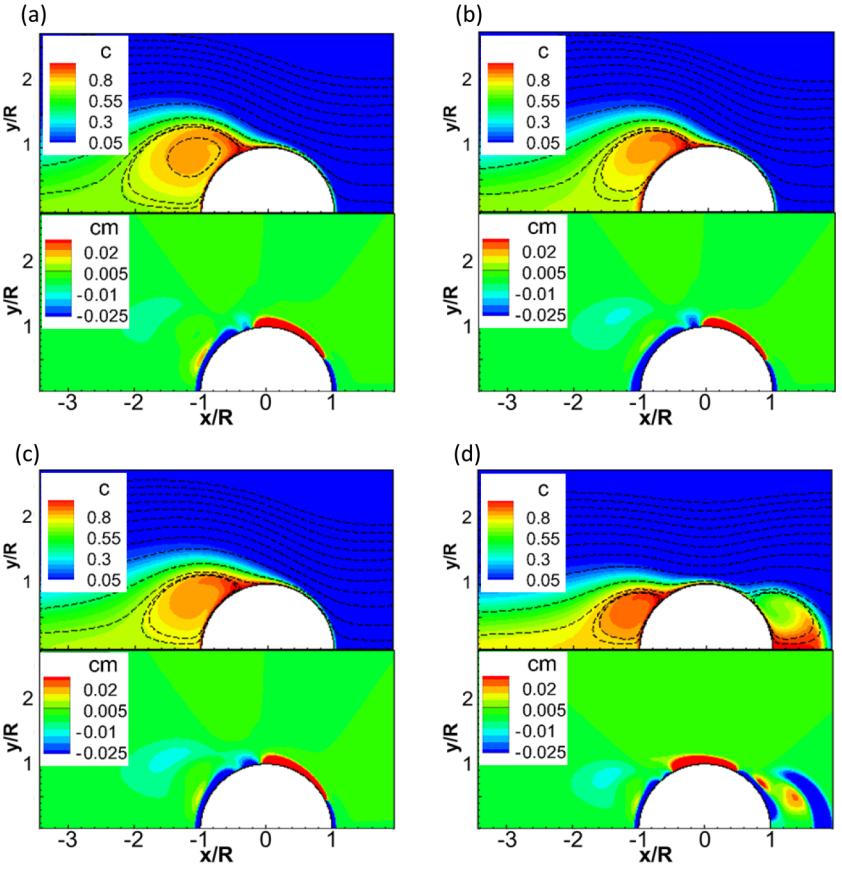

FIG. 10. Distributions of nutrient concentration (top) and its distributed effect on U_1/U_0 (bottom) for the minimum observed values in Fig. 7 assuming $\mathrm{Pe} = 400$ and $\xi = 1$: (a) point $(0.869, -0.328)$ in the β_2-β_3 plane for $U_1/U_0 = -0.097$, (b) point $(0.881, -0.276)$ in the β_2-β_4 plane for $U_1/U_0 = -0.090$, (c) point $(0.898, -0.1353)$ in the β_2-β_5 plane for $U_1/U_0 = -0.083$, and (d) point $(-0.920, -0.044)$ in the β_3-β_5 plane for $U_1/U_0 = -0.081$.

the swimmer. It reduces the size and strength of the regions with negative *cm* and enlarges regions with positive *cm* toward the front of the swimmer. By comparing the nutrient concentration contours of the cases with the maximum and minimum U_1/U_0, respectively, in Figs. 9 and 10, we can see that the changes in the surface stroke modes only marginally enhance the regions with negative *cm* compared to the pure treadmill case by thinning the boundary layer at the front and back of the swimmer ($\gamma > 0.4$ or $\gamma < -0.6$). The results show that the inclusion of higher modes in the surface motion of the swimmer serves an efficient local control mechanism to induce optimal stagnation points along the surface of the swimmer and enlarge the regions with a constructive *cm* value.

IV. CONCLUSION

In this study we explored the effects of nonuniform viscosity around a steady spherical squirmer on its swimming performance. The swimming stroke pattern of the squirmer surface was mathematically modeled as a series of Legendre polynomials which are normalized such that the total power expenditure by the swimmer is kept constant. An advection-diffusion equation was solved to determine the concentration of a nutrient around the squirmer and, through the relation between nutrient concentration and fluid viscosity, the pointwise viscosity was calculated. Finally, changes

in the swimming velocity of the squirmer in a fluid with nonuniform viscosity were related to the locomotion of the same body inside a fluid with constant viscosity.

It was shown that for the pure treadmill stroke, the first-order velocity change as a result of the nonuniform viscosity U_1/U_0 is finite and decreasing toward zero with increasing nutrient Péclet number. The numerical results were checked with the asymptotic analytical results at the limits of very large and very small Péclet numbers and good agreement was found.

When the surface motion of the squirmer is composed of higher strokes modes in addition to the pure treadmill stroke, negative U_1/U_0 is observed. In this situation, the change of the viscosity can cause either a decrease or an increase in the swimming velocity depending on both Péclet number and the nature of the relation between the nutrient concentration and viscosity change in the fluid. At high Péclet number, the appearance of the stagnation points along the surface of the squirmer as a result of higher stroke modes is found to reduce U_1/U_0. On the other hand, the presence of higher stroke modes can result in a thinner boundary layer in the front and back of the swimmer and an increase of U_1/U_0, especially along the intermediate surface between the tip of the swimmer and a limit point where the boundary layer separates the surface and depletes into a thin sheet behind the swimmer. At very small Péclet number, the diffusion process is dominant and the nutrient concentration is homogenized around the swimmer. Therefore, at low Pe any change in the surface stroke pattern does not result in substantial variation of U_1/U_0 due to the diffusion-dominated process smoothing out any effect of the boundary conditions.

There are several interesting observations to note from Fig. 4. First, for each stroke coupling, a peak, if it exists, occurs around $\mathrm{Pe} = O(1)$, after which the swimming performance monotonically decreases. This suggests that swimmers would prefer an environment that balances diffusion and advection processes and would possibly seek such an environment in order to maximize swimming performance. Second, not all stroke couples displayed this peak in performance, suggesting that the mode of swimming does matter. However, we note that for the parameter ranges observed the peak performance of coupled modes does not exceed the maxima for corresponding ξ for a pure treadmill stroke. This suggests that, for small variations in viscosity, the peak performance is still obtained by the pure treadmill stroke but it important to note that it no longer becomes a unique stroke combination that yields this peak performance.

The focus of this study was to investigate how the nonuniform change of viscosity around a microorganism can modify the swimming speed of a spherical squirmer with a steady surface stroke pattern. However, for a real fluid environment there is a coupling between the nutrient concentration and fluid field, whereas in the present study we only investigated the one-way influence of nutrient concentration on swimming velocity using the constant-viscosity stokes solution. This coupling could lead to larger effects which we have not been observed in the present study due to our assumption of a small dependence of the nutrient on viscosity. An investigation of this question using numerical techniques to model the Stokes flow around a sphere with nonuniform viscosity is beyond the scope of the present work. Also, the surface motion of a real swimmer consists of periodic strokes and further research is needed to understand the mechanism of viscosity change around an unsteady swimmer and how it affects the mean swimming velocity. It would also be interesting to study how the changes in the flow viscosity affect feeding performance of a swimmer, as in the uniform velocity case it has been shown that a pure treadmill stroke is optimal [13]. Moreover, quantification of this effect on other types of swimming modes that are routinely used by microorganisms is left for future work. Finally, in certain situations such as blood coagulation, the nonuniform viscosity is caused by the change in the rheology of the fluid or creation of multiscale elastic networks close to the surface of moving cells. The change of the viscosity near the body can be accompanied by changes in the viscoelasticity of the fluid as well as the changes in viscosity in shear-dependent non-Newtonian fluids. Further studies are required to fully understand this problem and determine whether modification of the nutrient gradient to create a phoresis effect is a viable swimming mechanism.

APPENDIX A: DERIVATION OF THE GENERALIZED RECIPROCAL THEOREM

To obtain the GRT relating our two domains, we follow previous results [50] and project the stress tensor of variable-viscosity flow onto an auxiliary Stokes flow with a constant viscosity of μ' around the same swimmer and use the incompressibility condition to obtain

$$\nabla \cdot (\mathbf{u}' \cdot \underline{\boldsymbol{\sigma}}) = 2\mu \nabla \mathbf{u}' : \underline{\boldsymbol{E}} + \mathbf{u}' \cdot \nabla \cdot \underline{\boldsymbol{\sigma}}, \tag{A1}$$

where a prime denotes the constant-viscosity field. Similarly, by interchanging the roles of two flow fields, the projection of the stress tensor of the auxiliary flow on the fluid velocity of the actual flow can be written as

$$\nabla \cdot (\mathbf{u} \cdot \underline{\boldsymbol{\sigma}}') = 2\mu' \nabla \mathbf{u} : \underline{\boldsymbol{E}}' + \mathbf{u} \cdot \nabla \cdot \underline{\boldsymbol{\sigma}}'. \tag{A2}$$

We can use the symmetry and zero trace of the rate of deformation tensor and write

$$\nabla \mathbf{u}' : \underline{\boldsymbol{E}} = \nabla \mathbf{u} : \underline{\boldsymbol{E}}' = \frac{1}{\mu} \nabla \mathbf{u}' : \underline{\boldsymbol{\sigma}} = \frac{1}{\mu'} \nabla \mathbf{u} : \underline{\boldsymbol{\sigma}}', \tag{A3}$$

and after subtracting Eq. (A2) from Eq. (A1), we can substitute Eq. (A3) and impose Eq. (1) for both actual and auxiliary flows to obtain

$$\nabla \cdot (\mathbf{u}' \cdot \underline{\boldsymbol{\sigma}} - \mathbf{u} \cdot \underline{\boldsymbol{\sigma}}') = \frac{\mu - \mu'}{\mu'} \nabla \mathbf{u} : \underline{\boldsymbol{\sigma}}'. \tag{A4}$$

Multiplying through by μ' and using the identity $\mathbf{u} \cdot \underline{A} \cdot \mathbf{v} = (\mathbf{u} \otimes \mathbf{v}) : \underline{A}$ for any vectors $\mathbf{u}$ and $\mathbf{v}$ and tensor $\underline{A}$, where $\otimes$ is the outer product, we can cancel one term to give

$$\mu'(\underline{\sigma} : \nabla \mathbf{u}') = \mu(\underline{\sigma}' : \nabla \mathbf{u}) \tag{A5}$$

or, equivalently,

$$\mu'(\nabla \cdot \underline{\sigma} \cdot \mathbf{u}') = \mu(\nabla \cdot \underline{\sigma}' \cdot \mathbf{u}), \tag{A6}$$

where we have dropped the outer product symbol for notational convenience, i.e., $\nabla \otimes \mathbf{u} \equiv \nabla \mathbf{u}$. Now applying the common identity $\nabla \cdot (g\mathbf{f}) = g\nabla \cdot \mathbf{f} + \nabla g \cdot \mathbf{f}$ for an arbitrary scalar function g and vector function $\mathbf{f}$, Eq. (A6)can be further simplified to

$$\nabla \cdot (\mu' \mathbf{u}' \cdot \underline{\boldsymbol{\sigma}} - \mu \mathbf{u} \cdot \underline{\boldsymbol{\sigma}}') = -\nabla \mu \cdot \underline{\boldsymbol{\sigma}}' \cdot \mathbf{u}. \tag{A7}$$

By integration of Eq. (A7) over the fluid domain V and applying divergence theorem, the integral form of Eq. (A7) can be expressed as

$$\iint_S (\mu' \mathbf{u}' \cdot \boldsymbol{\tau} - \mu \mathbf{u} \cdot \boldsymbol{\tau}') ds = \iiint_V \nabla \mu \cdot \underline{\boldsymbol{\sigma}}' \cdot \mathbf{u} \, dv, \tag{A8}$$

where for a free-swimming organism the first term on the left-hand side of Eq. (A8) is zero and the equation becomes

$$\iint_S \mu \mathbf{u} \cdot \boldsymbol{\tau}' ds = -\iiint_V \nabla \mu \cdot \underline{\boldsymbol{\sigma}}' \cdot \mathbf{u} \, dv, \tag{A9}$$

and with the substitution of Eq. (2) into Eq. (A9) we obtain

$$\iint_S \mu \mathbf{U} \cdot \boldsymbol{\tau}' ds + \iint_S \mu \Omega \cdot (\mathbf{x} \times \boldsymbol{\tau}') ds + \iint_S \mu \mathbf{u}^s \cdot \boldsymbol{\tau}' ds = -\iiint_V \nabla \mu \cdot \underline{\boldsymbol{\sigma}}' \cdot \mathbf{u} \, dv. \tag{A10}$$

It is the velocity fields in this equation that are expanded in a perturbation series to obtain the $O(\epsilon^0)$ and $O(\epsilon^1)$ results.

APPENDIX B: DEFINITIONS OF $A_i(m,n)$ AND $B_i(m,n)$

The coefficients of $A_i(m,n)$ and $B_i(m,n)$ in Eq. (24) are defined by the relations

$$A_i(m,n) = (2i+1)\frac{2n+1}{2}\int_{-1}^{1} P_i P_m P_n d\gamma, \tag{B1}$$

$$B_i(m,n) = (2i+1)\frac{2n+1}{2n(n+1)}\int_{-1}^{1} (1-\gamma^2) P_i P_m' P_n' d\gamma, \tag{B2}$$

where both $A_i(m,n)$ and $B_i(m,n)$ can be computed efficiently using their recursive relations as explained in [13].

APPENDIX C: ASYMPTOTIC FORMULATION OF THE CHANGES OF THE SWIMMING VELOCITY AT Pe $\ll$ 1

The asymptotic behavior of U_1/U_0 of a swimmer with the pure treadmill surface stroke at the limit of very low Pe is derived using the matched asymptotic expansion technique as explained previously by Michelin and Lauga [13]. To summarize, the domain is separated into near-field and far-field parts which overlap over a matching region. In the near-field $r = O(1)$, we can expand $c(r,\gamma)$ as a truncated power expansion of Pe around a swimmer,

$$c(r,\gamma) = c_0(r,\gamma) + \mathrm{Pe}\, c_1(r,\gamma) + \mathrm{Pe}^2 c_2(r,\gamma) + O(\mathrm{Pe}^3). \tag{C1}$$

The near-field expansion of $c(r,\gamma)$ satisfies advection-diffusion equation (21) as well as the Dirichlet boundary condition of $c = 1$ on the swimmer surface, which can be expressed explicitly as

$$\frac{1}{r^2}\left[\frac{\partial}{\partial r}\left(r^2\frac{\partial c}{\partial r}\right) + \frac{\partial}{\partial \gamma}\left((1-\gamma^2)\frac{\partial c}{\partial \gamma}\right)\right] = -\mathrm{Pe}\left[\gamma\left(1-\frac{1}{r^3}\right)\frac{\partial c}{\partial r} + \frac{1-\gamma^2}{r}\left(1+\frac{1}{2r^3}\right)\frac{\partial c}{\partial \gamma}\right]$$
$$\text{with } c = 1 \quad \text{at } r = 1. \tag{C2}$$

Similarly, the solution of the far field can be written as a boundary-layer solution derived from (21) with the change of variable of $\rho = (\mathrm{Pe})r$ along with the far-field boundary condition of $c \to 0$ for $\rho \to \infty$ and subsequently expanded as a regular perturbation series. By matching the power representations of c in near-field and far-field subdomains over the region of $\mathrm{Pe}^{-2/3} \ll r \ll \mathrm{Pe}^{-1}$, one can obtain the final solution of $c(r,\gamma)$ in the region of $r \ll \mathrm{Pe}^{-1}$ as

$$c(r,\gamma) = \frac{1}{r} + \sum_{p=1}^{2} \mathrm{Pe}^p \sum_{q=0}^{p} c_p^q(r) P_q(\gamma), \tag{C3}$$

where c_p^q are given in [13].

A similar procedure can be taken to calculate the series expansion of $c(\rho,\gamma)$ in the far field. Since the volume integral in Eq. (14) primarily depends on the $c(\rho,\gamma)$ distribution in the near field and the effect of its distribution in the far field is negligible, the near-field solution is only used to examine the change in the summing velocity. For further details, refer to [13]. Here, by substituting Eq. (C3) in Eq. (5) and using Eq. (14), we can find analytical expressions of U_1/U_0, which for $\xi = 1.0$ and 2.0 are

$$\frac{U_1}{U_0} = \begin{cases} 0.083 + 0.042\,\mathrm{Pe} - 0.05\,\mathrm{Pe}^2 + O(\mathrm{Pe}^3) & \text{if } \xi = 1 \\ 0.11 + 0.031\,\mathrm{Pe} - 0.067\,\mathrm{Pe}^2 + O(\mathrm{Pe}^3) & \text{if } \xi = 2. \end{cases} \tag{C4}$$

APPENDIX D: ASYMPTOTIC FORMULATION OF THE SWIMMING VELOCITY AT Pe $\gg$ 1

When the Pe is high, the nutrient concentrates in a thin boundary layer along the surface of a squirmer and a boundary-layer formulation can be used to described its distribution around the

swimmer [12,13]. Since the tangential velocity of the swimmer surface is $O(1)$, the boundary-layer thickness changes as $\sqrt{\mathrm{Pe}}$ as a result of mass transfer of a nutrient in the radial and tangential directions. To estimate the boundary-layer thickness, we define

$$Y = \sqrt{\mathrm{Pe}}(r-1). \tag{D1}$$

Substituting Eq. (D1) in Eq. (21) and retaining only the dominant terms with the leading order of $1/\sqrt{\mathrm{Pe}}$, the boundary-layer equation can be expressed as

$$\frac{\partial^2 c}{\partial Y^2} = Y\left(\sqrt{1-\gamma^2}\frac{du_\theta^s}{d\gamma} - \frac{\gamma}{\sqrt{1-\gamma^2}}u_\theta^s\right)\frac{\partial c}{\partial Y} - \sqrt{1-\gamma^2}u_\theta^s\frac{\partial c}{\partial \gamma}. \tag{D2}$$

Assuming only treadmill motion (i.e., $\beta_i = 0$ if $i \neq 1$), the surface velocity is $u_\theta^s(\gamma) = \sqrt{\frac{3}{2}}\beta_1\sqrt{1-\gamma^2}$ and Eq. (D2) can be further simplified to

$$\frac{\partial^2 c}{\partial Y^2} = -\sqrt{\frac{3}{2}}\beta_1\left[2\gamma Y\frac{\partial c}{\partial Y} + (1-\gamma^2)\frac{\partial c}{\partial \gamma}\right]. \tag{D3}$$

By defining a similarity variable $\zeta = Y/g(\gamma)$ (Y is the scaled coordinate along r and $g(\gamma)$ represents the change of boundary-layer thickness along γ), we can transform the partial differential equation (D3) to an ordinary differential equation with respect to ζ as

$$\frac{\partial^2 c}{\partial \zeta^2} - \sqrt{\frac{3}{2}}\beta_1\left[2\gamma g^2 + \frac{1-\gamma^2}{2}(g^2)'\right]\frac{\partial c}{\partial \zeta} = 0. \tag{D4}$$

The self-similar solution that is also compatible with the boundary conditions (22) can be obtained only if $g(\gamma)$ satisfies

$$2\gamma g^2 + \frac{1-\gamma^2}{2}(g^2)' = -2\sqrt{\frac{2}{3}}\beta_1, \tag{D5}$$

which results in the following expression for c:

$$c(Y,\gamma) = \mathrm{erfc}\left(\frac{Y}{g(\gamma)}\right). \tag{D6}$$

Taking into account that the boundary-layer thickness is finite at the front point $\gamma = 1$, the solution of $g(\gamma)$ can be computed from Eq. (D5) and expressed as

$$g(\gamma) = \frac{2}{\sqrt{3\sqrt{\frac{3}{2}}\beta_1}}\frac{\sqrt{\gamma+2}}{\gamma+1}. \tag{D7}$$

Finally, with the substitution of Eq. (D6) in Eq. (5) and using the result to calculate the integral (14), the asymptotic value of U_1/U_0 at the limit of high Péclet number can be computed. At very high Péclet number, it can be shown that $\lim_{\mathrm{Pe}\to\infty} U_1/U_0 = 0$ for all ξ values.

[1] D. Bray, *Cell Movements: From Molecules to Motility* (Garland Science, New York, 2001).

[2] C. Brennen and H. Winet, Fluid mechanics of propulsion by cilia and flagella, Annu. Rev. Fluid Mech. **9**, 339 (1977).

[3] L. J. Fauci and R. Dillon, Biofluidmechanics of reproduction, Annu. Rev. Fluid Mech. **38**, 371 (2006).

[4] J. Lighthill, *Mathematica Biofluiddynamics* (Society for Industrial and Applied Mathematics, Philadelphia, 1975).

[5] S. Childress, *Mechanics of Swimming and Flying* (Cambridge University Press, Cambridge, 1981), Vol. 2.

[6] E. Lauga and T. R. Powers, The hydrodynamics of swimming microorganisms, Rep. Prog. Phys. **72**, 096601 (2009).

[7] E. M. Purcell, Life at low Reynolds number, Am. J. Phys. **45**, 3 (1977).
[8] B. Baccetti, Insect sperm cells, Adv. Insect Physiol. **9**, 315 (1972).
[9] H. C. Berg, The rotary motor of bacterial flagella, Biochemistry **72**, 19 (2003).
[10] R. Rikmenspoel and C. A. Isles, Digitized precision measurements of the movements of sea urchin sperm flagella, Biophys. J. **47**, 395 (1985).
[11] S. Childress, M. Koehl, and M. Miksis, Scanning currents in Stokes flow and the efficient feeding of small organisms, J. Fluid Mech. **177**, 407 (1987).
[12] V. Magar, T. Goto, and T. Pedley, Nutrient uptake by a self-propelled steady squirmer, Q. J. Mech. Appl. Math. **56**, 65 (2003).
[13] S. Michelin and E. Lauga, Optimal feeding is optimal swimming for all Péclet numbers, Phys. Fluids **23**, 101901 (2011).
[14] M. B. Short, C. A. Solari, S. Ganguly, T. R. Powers, J. O. Kessler, and R. E. Goldstein, Flows driven by flagella of multicellular organisms enhance long-range molecular transport, Proc. Natl. Acad. Sci. USA **103**, 8315 (2006).
[15] K. J. Niklas, *Plant Allometry: The Scaling of Form and Process* (University of Chicago Press, Chicago, 1994).
[16] P. S. Lovely and F. Dahlquist, Statistical measures of bacterial motility and chemotaxis, J. Theor. Biol. **50**, 477 (1975).
[17] D. W. Crawford and D. A. Purdie, Evidence for avoidance of flushing from an estuary by a planktonic, phototrophic ciliate, Mar. Ecol. Prog. Ser. **79**, 259 (1992).
[18] T. Fenchel, Microbial behavior in a heterogeneous world, Science **296**, 1068 (2002).
[19] R. Stocker, J. R. Seymour, A. Samadani, D. E. Hunt, and M. F. Polz, Rapid chemotactic response enables marine bacteria to exploit ephemeral microscale nutrient patches, Proc. Natl. Acad. Sci. USA **105**, 4209 (2008).
[20] S. Michelin and E. Lauga, Phoretic self-propulsion at finite Péclet numbers, J. Fluid Mech. **747**, 572 (2014).
[21] O. S. Beveridge, O. L. Petchey, and S. Humphries, Direct and indirect effects of temperature on the population dynamics and ecosystem functioning of aquatic microbial ecosystems, Adv. Insect Physiol. **79**, 1324 (2010).
[22] H. Winet, Ciliary propulsion of objects in tubes: Wall drag on swimming tetrahymena (ciliata) in the presence of mucin and other long-chain polymers, J. Exp. Biol. **64**, 283 (1976).
[23] J. Feng and S. K. Cho, Mini and micro propulsion for medical swimmers, Micromachines **5**, 97 (2014).
[24] J. Anderson, M. Lowell, and D. Prieve, Motion of a particle generated by chemical gradients. Part 1. Non-electrolytes, J. Fluid Mech. **117**, 107 (1982).
[25] R. Golestanian, T. Liverpool, and A. Ajdari, Designing phoretic micro-and nano-swimmers, New J. Phys. **9**, 126 (2007).
[26] M. M. Hanczyc, T. Toyota, T. Ikegami, N. Packard, and T. Sugawara, Fatty acid chemistry at the oil-water interface: Self-propelled oil droplets, J. Am. Chem. Soc. **129**, 9386 (2007).
[27] S. Herminghaus, C. C. Maass, C. Krüger, S. Thutupalli, L. Goehring, and C. Bahr, Interfacial mechanisms in active emulsions, Soft Matter **10**, 7008 (2014).
[28] Z. Izri, M. N. van der Linden, S. Michelin, and O. Dauchot, Self-Propulsion of Pure Water Droplets by Spontaneous Marangoni-Stress-Driven Motion, Phys. Rev. Lett. **113**, 248302 (2014).
[29] T. Toyota, N. Maru, M. M. Hanczyc, T. Ikegami, and T. Sugawara, Self-propelled oil droplets consuming "fuel" surfactant, J. Am. Chem. Soc. **131**, 5012 (2009).
[30] E. Lauga and A. M. Davis, Viscous Marangoni propulsion, J. Fluid Mech. **705**, 120 (2012).
[31] H. Masoud and H. A. Stone, A reciprocal theorem for Marangoni propulsion, J. Fluid Mech. **741**, R4 (2014).
[32] V. Vandadi, S. J. Kang, and H. Masoud, Reverse Marangoni surfing, J. Fluid Mech. **811**, 612 (2017).
[33] A. Würger, Thermally driven Marangoni surfers, J. Fluid Mech. **752**, 589 (2014).
[34] J. Gachelin, G. Mino, H. Berthet, A. Lindner, A. Rousselet, and É. Clément, Non-Newtonian Viscosity of *Escherichia Coli* Suspensions, Phys. Rev. Lett. **110**, 268103 (2013).
[35] H. M. López, J. Gachelin, C. Douarche, H. Auradou, and E. Clément, Turning Bacteria Suspensions into Superfluids, Phys. Rev. Lett. **115**, 028301 (2015).

[36] M. Dasgupta, B. Liu, H. C. Fu, M. Berhanu, K. S. Breuer, T. R. Powers, and A. Kudrolli, Speed of a swimming sheet in Newtonian and viscoelastic fluids, Phys. Rev. E **87**, 013015 (2013).
[37] M. De Corato and G. D'Avino, Dynamics of a microorganism in a sheared viscoelastic liquid, Soft Matter **13**, 196 (2017).
[38] E. Lauga, Locomotion in complex fluids: Integral theorems, Phys. Fluids **26**, 081902 (2014).
[39] H. Nganguia, K. Pietrzyk, and O. S. Pak, Swimming efficiency in a shear-thinning fluid, Phys. Rev. E **96**, 062606 (2017).
[40] Y. Zhang, G. Li, and A. M. Ardekani, Reduced viscosity for flagella moving in a solution of long polymer chains, Phys. Rev. Fluids **3**, 023101 (2018).
[41] A. Sokolov and I. S. Aranson, Reduction of Viscosity in Suspension of Swimming Bacteria, Phys. Rev. Lett. **103**, 148101 (2009).
[42] J. Celli, B. Turner, N. Afdhal, S. Keates, I. Ghiran, C. Kelly, R. Ewoldt, G. McKinley, P. So, S. Erramilli, and R. Bansil, *Helicobacter pylori* moves through mucus by reducing mucin viscoelasticity, Proc. Natl. Acad. Sci. USA **106**, 14321 (2009).
[43] S. A. Mirbagheri and H. C. Fu, *Helicobacter pylori* Couples Motility and Diffusion to Actively Create a Heterogeneous Complex Medium in Gastric Mucus, Phys. Rev. Lett. **116**, 198101 (2016).
[44] B. Brahamsha, Non-flagellar swimming in marine *Synechococcus*, J. Mol. Microbiol. Biotechnol **1**, 59 (1999).
[45] K. Ehlers and G. Oster, On the mysterious propulsion of *Synechococcus*, PLoS ONE **7**, e36081 (2012).
[46] K. M. Ehlers and J. Koiller, Could cell membranes produce acoustic streaming? Making the case for *Synechococcus* self-propulsion, Math. Comput. Model. **53**, 1489 (2011).
[47] K. M. Ehlers, A. Samuel, H. C. Berg, and R. Montgomery, Do cyanobacteria swim using traveling surface waves? Proc. Natl. Acad. Sci. USA **93**, 8340 (1996).
[48] T. P. Pitta and H. C. Berg, Self-electrophoresis is not the mechanism for motility in swimming cyanobacteria, J. Bacteriol. **177**, 5701 (1995).
[49] J. Elgeti, R. G. Winkler, and G. Gompper, Physics of microswimmers-single particle motion and collective behavior: A review, Rep. Prog. Phys. **78**, 056601 (2015).
[50] C. Pozrikidis, Reciprocal identities and integral formulations for diffusive scalar transport and Stokes flow with position-dependent diffusivity or viscosity, J. Eng. Math. **96**, 95 (2016).
[51] M. N. Moore and M. J. Shelley, A weak-coupling expansion for viscoelastic fluids applied to dynamic settling of a body, J. Non-Newtonian Fluid Mech. **183-184**, 25 (2012).
[52] N. Oppenheimer, S. Navardi, and H. A. Stone, Motion of a hot particle in viscous fluids, Phys. Rev. Fluids **1**, 014001 (2016).
[53] C. Pozrikidis, *Boundary Integral and Singularity Methods for Linearized Viscous Flow* (Cambridge University Press, Cambridge, 1992).
[54] R. Cortez, The method of regularized Stokeslets, SIAM J. Sci. Comput. **23**, 1204 (2001).
[55] J. B. Keller and S. I. Rubinow, Slender-body theory for slow viscous flow, J. Fluid Mech. **75**, 705 (1976).
[56] A. T. Chwang and T. Wu, Hydromechanics of low-Reynolds-number flow. Part 2. Singularity method for Stokes flows, J. Fluid Mech. **67**, 787 (1975).
[57] J. Blake, A spherical envelope approach to ciliary propulsion, J. Fluid Mech. **46**, 199 (1971).
[58] M. Lighthill, On the squirming motion of nearly spherical deformable bodies through liquids at very small Reynolds numbers, Commun. Pure Appl. Math. **5**, 109 (1952).
[59] T. Ishikawa, M. Simmonds, and T. Pedley, Hydrodynamic interaction of two swimming model micro-organisms, J. Fluid Mech. **568**, 119 (2006).
[60] Z. Lin, J.-L. Thiffeault, and S. Childress, Stirring by squirmers, J. Fluid Mech. **669**, 167 (2011).
[61] S. Wang and A. Ardekani, Inertial squirmer, Phys. Fluids **24**, 101902 (2012).
[62] Z. Zhang and A. Prosperetti, A second-order method for three-dimensional particle simulation, J. Comput. Phys. **210**, 292 (2005).
[63] H. A. Stone and A. D. Samuel, Propulsion of Microorganisms by Surface Distortions, Phys. Rev. Lett. **77**, 4102 (1996).
[64] S. Dennis, J. Walker, and J. Hudson, Heat transfer from a sphere at low Reynolds numbers, J. Fluid Mech. **60**, 273 (1973).